Gas phase structures and charge localization in small aluminum oxide anions: Infrared photodissociation spectroscopy and electronic structure calculations

Xiaowei Song,[1,2] Matias R. Fagiani,[1,2] Sandy Gewinner,[1] Wieland Schöllkopf,[1] Knut R. Asmis,[2,a)] Florian A. Bischoff,[3] Fabian Berger,[3] and Joachim Sauer[3,a)]
[1]*Fritz-Haber-Institut der Max-Planck-Gesellschaft, Faradayweg 4-6, D-14195 Berlin, Germany*
[2]*Wilhelm-Ostwald-Institut für Physikalische und Theoretische Chemie, Universität Leipzig, Linnéstrasse 2, D-04103 Leipzig, Germany*
[3]*Institut für Chemie, Humboldt-Universität zu Berlin, Unter den Linden 6, D-10099 Berlin, Germany*

(Received 8 April 2016; accepted 6 June 2016; published online 27 June 2016)

We use cryogenic ion trap vibrational spectroscopy in combination with quantum chemical calculations to study the structure of mono- and dialuminum oxide anions. The infrared photodissociation spectra of D_2-tagged $AlO_{1\text{-}4}^-$ and $Al_2O_{3\text{-}6}^-$ are measured in the region from 400 to 1200 cm^{-1}. Structures are assigned based on a comparison to simulated harmonic and anharmonic IR spectra derived from electronic structure calculations. The monoaluminum anions contain an even number of electrons and exhibit an electronic closed-shell ground state. The $Al_2O_{3\text{-}6}^-$ anions are oxygen-centered radicals. As a result of a delicate balance between localization and delocalization of the unpaired electron, only the BHLYP functional is able to qualitatively describe the observed IR spectra of all species with the exception of AlO_3^-. Terminal Al–O stretching modes are found between 1140 and 960 cm^{-1}. Superoxo and peroxo stretching modes are found at higher (1120-1010 cm^{-1}) and lower energies (850-570 cm^{-1}), respectively. Four modes in-between 910 and 530 cm^{-1} represent the IR fingerprint of the common structural motif of dialuminum oxide anions, an asymmetric four-member Al–$(O)_2$–Al ring. *Published by AIP Publishing.* [http://dx.doi.org/10.1063/1.4954158]

I. INTRODUCTION

Aluminum oxides are widely used as ceramics, coatings, abrasives, adsorbents as well as components of solid catalysts.[1] For such complex materials, it remains difficult to characterize or predict the molecular scale properties and structures with atomic resolution. Gas-phase clusters, in contrast, are amenable to highly sensitive and selective experimental techniques as well as higher level computational methods. Experiments on these model systems thus provide insight into structure-reactivity correlations as well as the transition from molecular to condensed phase properties.[2–4] Small aluminum oxide cluster cations[5,6] and anions[7] containing oxygen-centered radicals have raised interest recently as models for understanding water chemisorption and C–H bond activation. There is also an astrochemical interest in the role that small aluminum oxide clusters play in the formation of circumstellar corundum (Al_2O_3) grains.[8]

In the present study, we use cryogenic ion trap vibrational spectroscopy of messenger-tagged, mass-selected anions in combination with density functional theory (DFT) to examine the geometric structure of $AlO_{1\text{-}4}^-$ and $Al_2O_{3\text{-}6}^-$ ions formed by sputtering of elemental aluminum in the presence of oxygen. We are particularly interested in the identification of reactive oxygen species like $O_2^{-\cdot}$ (superoxo), O_2^{2-} (peroxo), and $O^{-\cdot}$ (atomic oxygen radicals). The computed structures of the aluminum oxide clusters containing oxygen-centered radicals sensitively depend on the amount of exact exchange mixed into the exchange-correlation functional. Moreover, anharmonic effects, like Fermi resonances, prove to be important for explaining the experimental IR spectra.

Previous mass spectrometric investigations on gas phase aluminum oxide cluster ions have focused on their reactivity towards water,[6,9] carbon monoxide,[10] ammonia,[11] methane,[5,6] and larger alkanes.[7] The smaller anions show a variety of reactions, but react more selectively than the corresponding cations. The electronically closed-shell AlO_2^- ion readily adsorbs two water molecules forming $Al(OH)_4^-$ in a barrierless reaction.[9] $Al_2O_3^-$ and $Al_2O_4^-$ react with CO under atomic oxygen loss, suggesting the formation of CO_2.[10] In $Al_2O_4^-$ and $Al_2O_6^-$, the atomic oxygen radical is predicted to be the active site for hydrogen atom abstraction from *n*-butane.[7] Mass spectrometry has also been used to determine ionization energies by the way of bracketing experiments.[12]

Less is known about the vibrational spectroscopy of small aluminum oxide clusters. Matrix isolation IR spectroscopy has been used to study neutral clusters up to AlO_6 and Al_2O_3.[13–16] Aluminum oxide anions up to $Al_7O_5^-$ have been studied using anion photoelectron (APE) spectroscopy.[17–21] The APE spectra of the smaller anions are vibrationally resolved, and when combined with electronic structure calculations, they allowed identifying an Al–$(O)_2$–Al rhombus as a common structural motif of small neutral and anionic dinuclear aluminum oxides.[18] Recently, vibrational and rotational molecular constants of AlO^- were determined by means of autodetachment spec-

a)Authors to whom correspondence should be addressed. Electronic addresses: knut.asmis@uni-leipzig.de and js@chemie.hu-berlin.de.

troscopy.[22] Detailed structural information on gas phase clusters can be obtained from infrared photodissociation (IRPD) spectroscopy, but until now IRPD spectra have only been reported for the aluminum oxide cations $[(Al_2O_3)_{1\text{-}4}(AlO)]^+$.[23]

Electronic structure studies on smaller aluminum oxides containing up to two Al atoms have focused mainly on neutral[24–34] and to a lesser extent on anionic[7,26,27,35–37] clusters. For AlO^-, AlO_2^-, and AlO_4^-, closed-shell electronic ground states of $^1\Sigma^+$ ($C_{\infty v}$), $^1\Sigma_g$ ($D_{\infty h}$), and $^1A_1$ (D_{2d}) symmetry, respectively, have been predicted.[26,27,36] Dialuminum oxide anions, $Al_2O_n^-$, contain an uneven number of electrons and, for n = 2-6, are characterized by a rhombic Al–$(O)_2$–Al structural motif.[7,35] The unpaired electron is found to be localized on one of the two terminal O-atoms in $Al_2O_4^-$ (C_{2v} structure), while in $Al_2O_6^-$ it is delocalized equally over the two terminal η^2-O_2 groups (D_{2h} structure).[7]

II. EXPERIMENTAL METHODS

Infrared photodissociation experiments are conducted on an ion trap tandem mass spectrometer described elsewhere.[38] Briefly, aluminum oxide anions are generated using a magnetron sputtering source.[39] Compared to more commonly used laser ablation sources, this source often yields higher ion signals for smaller metal oxide ions ($\lesssim$10 atoms). Continuous flows of Ar and O_2 buffer gases are injected in front of the Al-sputtering target. He gas is introduced from the back of the sputtering chamber. The partial pressures inside the sputtering chamber are controlled individually by mass-flow controllers and allow optimizing the cluster composition and size distribution (see Fig. S1 in the supplementary material[40] for a typical quadrupole mass spectrum). Typically, the O_2 to Ar flow-ratio is below 10% and the total flow results in a pressure up to 10^{-3} mbar in the source chamber. Clusters nucleate and grow in a cooled aggregation chamber held at temperatures between 100 and 200 K. The distance between the sputter head and the source chamber nozzle (10-25 cm) is optimized for best signal. The cluster beam is collimated using a 4 mm diameter skimmer. Subsequently, negative ions are compressed in phase using a radio-frequency (RF) decapole ion-guide filled with He as buffer gas and mass-selected using a quadrupole mass-filter. Mass-selected anions are deflected by 90° and focused into a RF linear ring-electrode ion-trap held at cryogenic temperatures (15-19 K) and continuously filled with D_2 gas. Trapped ions are accumulated and internally cooled by collisions with the D_2 gas. Aluminum oxide anions are messenger-tagged with D_2 via three-body collisions: $Al_{1,2}O_n^- + 2D_2 \rightarrow Al_{1,2}O_n^-{\cdot}D_2 + D_2$. After an ion trap fill time of 199 ms, all ions are extracted from the ion trap and are focused in the center of the extraction region of a time-of-flight (TOF) mass spectrometer. There they are irradiated by an intense and wavelength-tunable IR laser pulse. When resonant with a vibrational transition, parent ions absorb a photon and eventually lose one or more messenger molecules via intramolecular vibrational predissociation.

The intense and tunable IR pulses are generated by the Fritz-Haber-Institute free-electron laser (FHI FEL).[41] The wavelength of the IR radiation is tuned from 8 to 25 μm with a bandwidth of ca. 0.2% root-mean-square (rms) of the central wavelength and pulse energies of ~0.5–14 mJ. IR spectra are recorded by averaging over 60 TOF mass spectra per wavelength step. The intensities are normalized to the total number of parent and fragment ions, to account for fluctuations in the total ion signal. Typically, a distribution of $(D_2)_m$-tagged anions, peaking at m = 1 and extending up to m = 4, were produced in the ion trap. However, the differences between the action spectra of anions with a single (m = 1) and with more than one tag (m > 1) were negligible (see Fig. S2 in the supplementary material[40]) and therefore the ion yields of all tagged anions were summed up for determining the parent ion yield. The IRPD cross section σ is determined as described previously.[42]

III. COMPUTATIONAL METHODS

For DFT structure prediction, the potential energy surface (PES) is searched first for the global minimum structures with a genetic algorithm[43,44] using the BP86 functional[45,46] together with the split-valence polarized basis set SVP[47] (denoted BP86/SVP). The genetic algorithm run is repeated three times for 500 structures, after which convergence is checked. Then, the ten lowest energy structures of the GA run are refined using the B3LYP[48] functional with the TZVPP[47] basis set (Al: 5s5p3d1f, O: 5s3p2d1f). These basis sets, denoted "def2" in the Turbomole library,[49] are sufficiently diffuse and, hence, adequate for a study on metal oxide anions. Finally, the structures are reoptimized using BHLYP[50]/TZVPP which includes 50% Fock exchange in the exchange-correlation functional. For the smaller AlO_n^- systems, the coupled cluster singles and doubles with perturbative triples method CCSD(T) (see Ref. 51 and references therein) with the aug-cc-pwCVTZ[52] basis set and frozen core orbitals are also applied. Closed-shell anions were computed in the spin-restricted formalism of the respective theories, open-shell species in the spin-unrestricted formalism (DFT) and ROHF/UCCSD(T) formalism (CCSD(T)). The dodo program[53] is used for the genetic algorithm.

Unless explicitly stated otherwise, IR spectra are computed within the double harmonic approximation. Anharmonic corrections to the vibrational energies including Fermi resonances were computed as implemented in Gaussian 09.[54] Simulated harmonic spectra are derived from computed stick spectra and convoluted with a 10 cm^{-1} full width at half maximum (FWHM) Gaussian line shape function to effectively account for rotational band contours and the spectral width of the laser pulse.

Electronic structure calculations are performed using the following program packages: MOLPRO 2012 (Coupled-Cluster),[55] Turbomole (DFT structure optimization and harmonic frequencies),[49] and Gaussian 09 (DFT anharmonicities).[56] Total energies and x, y, z coordinates for the BHLYP-optimized structures are given in the supplementary material.[40]

IV. RESULTS AND DISCUSSION

A. Experimental results

IRPD spectra of D_2-tagged $AlO_{1\text{-}4}^-$ and $Al_2O_{3\text{-}6}^-$ anions, measured in the spectral range from 400 to 1200 cm^{-1}

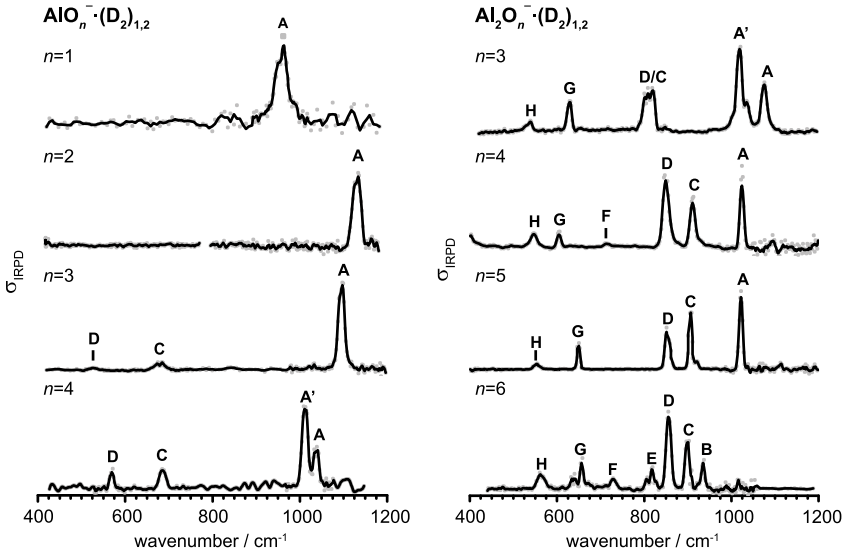

FIG. 1. IRPD spectra of D_2-tagged $AlO_{1\text{-}4}^-$ (left) and $Al_2O_{3\text{-}6}^-$ (right) in the spectral range from 400 to 1200 cm^{-1}. The raw data (gray dots) and the three point adjacent-averaged trace (solid line) are plotted. Spectral features are labeled with capital letters. See Tables I and II for band positions and assignments.

and monitoring the D_2 loss channels, are shown in Fig. 1. Spectral features are labeled with capital letters from A-H. Experimental band positions are summarized in Tables I and II.

1. Monoaluminum oxide anions

The IRPD spectrum of D_2-tagged AlO^- exhibits a single band, labeled **A** in Fig. 1, with a FWHM of 31 cm^{-1} and a rotational envelope characteristic of a linear rotor. Simulation of the rotational band contour yields a band origin of 957 cm^{-1} and rotational temperature of ~50 K. This band corresponds to excitation of the Al–O stretching fundamental (ν), in agreement with the value of 953.7 cm^{-1} for bare AlO^- in its $^1\Sigma^+$ ground state determined from autodetachment spectroscopy.[22] In the isoelectronic SiO ($^1\Sigma^+$) this band is observed 225 cm^{-1} higher in energy at 1182 cm^{-1}.[57]

The experimental IRPD spectrum of D_2-tagged AlO_2^- exhibits a single band at 1134 cm^{-1} (**A**), blue-shifted by 177 cm^{-1} with respect to band **A** in the AlO^- spectrum. This blue shift is comparable to that observed in the IR spectra of SiO_2 (versus SiO) of 198 cm^{-1}, where the band at 1380 cm^{-1} corresponds to the antisymmetric stretch fundamental ν_{AS} of linear silicon dioxide.[57] Hence, band **A** is assigned to the ν_{AS} mode of a linear O–Al–O structure, similar to the ground state structures reported for the analog group III oxides BO_2^- and GaO_2^-.[58,59] A linear structure was also derived from APE spectra, which reveal the IR-inactive symmetric stretching mode in the form of a hot band at 680 ± 60 cm^{-1}.[17]

The IRPD spectrum of D_2-tagged AlO_3^- looks similar to that of AlO_2^- in that it is also dominated by an intense band at high energies (**A**, 1098 cm^{-1}), indicating the presence of terminal metal-oxo bonds. In addition, two weaker bands are observed at lower energies at ~680 (**C**) and 526 cm^{-1} (**D**). The isoelectronic silicon trioxide exhibits a closed-shell singlet ground state with a planar C_{2v} structure that contains a strained SiO_2 ring.[60,61] The IR spectrum of SiO_3 is characterized by a dominant peak at high energies (1364 cm^{-1}), 16 cm^{-1} below the corresponding intense absorption in SiO_2 (1380 cm^{-1}), and

TABLE I. Experimental and calculated harmonic vibrational frequencies (in cm^{-1}) of $AlO_{1\text{-}4}^-$, including main contributions of local modes and irreducible representations (irrep) of the delocalized normal modes.

Species	Mode	Band	Expt.	Irrep	B3LYP	BHLYP[a]	BHLYP (scaled)[b]	CCSD(T)
AlO^-	ν (AlO)	A	957	σ	977	1041 (83)	971	953
AlO_2^-	ν_{AS} (OAlO)	A	1134	σ_u	1131	1242 (160)	1159	1127
	ν_S (OAlO)			σ_g	784	866 (0)	809	786
AlO_3^-	ν (AlO)	A	1098	a_1	1116	1179 (204)	1101	1094
	$\nu(O_2^{2-})$	B	842	a_1	801	878 (1)	820	742
	$\nu_{AS}(AlO_2)$	C	685/675	b_1	662	693 (25)	647	670
	$\nu_S(AlO_2)$	D	526	a_1	586	642 (20)	598	538
AlO_4^-	$\nu_S(AlO_2^{sym.\ str.}) + \nu_{AS}(O_2^{str.})$	A	1039	$a_1 + b_2$				1063[c]
	$\nu_{AS}(AlO_2^{sym.\ str.})$	A′	1011	b_2	1040	1102 (228)	1029	1021
	$\nu_{AS}(AlO_2)$	C	685	e	675	705 (26)	659	683
	$\nu_{AS}(O_2^{str.})$	D	572	b_2	683	766 (57)	716	587

[a]IR intensities (in km/mol) are listed in parentheses.
[b]Scaled with 0.9339, taken from Table II of Ref. 73.
[c]Sum of frequencies: 476 cm^{-1} (a_1, $\nu_S(AlO_2^{sym.\ str.})$) and 587 cm^{-1} (b_2, $\nu_{AS}(O_2^{str.})$).

TABLE II. Experimental and calculated harmonic vibrational frequencies (in cm^{-1}) of $Al_2O_{3\text{-}6}^-$, including main contributions of local modes and irreducible representations (irrep) of the delocalized normal modes.

Species	Mode	Band	Expt.	Irrep	BHLYP	BHLYP (scaled)[a]
$Al_2O_3^-$	ν (AlO)	A	1076	a_1	1099[b]	1026
	$2\nu_{AS,2}$ (ring)	A′	1019		1127[b]	1053
	$\nu_{S,1}$ (ring), $\nu_{AS,1}$ (ring)	C/D	818/800	a_1/b_1	866/848	809/791
	$\nu_{S,2}$ (ring)	G	629	a_1	667	623
	$\nu_{AS,2}$ (ring)	H	539	b_1	564	527
$Al_2O_4^-$	ν (AlO)	A	1024	a_1	1108	1035
	ν (AlO)	C	913	a_1	979	914
	$\nu_{AS,1}$ (ring)	D	850	b_1	903	843
	$\nu_{S,1}$ (ring)	F	715	a_1	748	699
	$\nu_{S,2}$ (ring)	G	606	a_1	642	600
	$\nu_{AS,2}$ (ring)	H	546	b_1	574	535
$Al_2O_5^-$	$\nu(O_2^-)$	*	1113	a_1	1288	1202
	ν (AlO)	A	1022	a_1	1107	1032
	$\nu_{S,1}$ (ring)	C	907/921	a_1	947	884
	$\nu_{AS,1}$ (ring)	D	851	b_1	905	844
	$\nu_{S,2}$ (ring)	G	650	a_1	692	645
	$\nu_{AS,2}$ (ring)	H	554	b_1	581	542
$Al_2O_6^-$	$\nu(O_2^-)$	*	1016	a_1	1287	1202
	ν (Al–O_2^{2-})	B	937	a_1	1008	941
	$\nu_{S,1}$ (ring)	C	900	a_1	943	881
	$\nu_{AS,1}$ (ring)	D	855	b_1	903	842
		E	819/807			
	$\nu(O_2^{2-})$	F	729	a_1	777	726
	$\nu_{AS,2}$ (OAlO)			b_2	701	655
	$\nu_{S,2}$ (ring)	G	640	a_1	694	648
	$\nu_{AS,2}$ (ring)	H	560	b_1	597	558

[a]Scaled with 0.9339, taken from Table II of Ref. 73.
[b]Anharmonic BHLYP frequencies: 1089 and 1046 cm^{-1} (Fermi resonance).

two weaker absorptions roughly 500 cm^{-1} lower in energy at 877 and 855 cm^{-1}. This compares favorably with the present IRPD spectrum of AlO_3^-, which is characterized by a red shift of the most intense absorption (versus AlO_2^-) of 36 cm^{-1} and considerably weaker features ~420 cm^{-1} lower in energy, indicating a similar geometric arrangement as in SiO_3. A C_{2v} structure with a peroxo-group as part of a three-membered ring has also been predicted for the ground state of GaO_3^-.[62]

Finally, the IRPD spectrum of D_2-tagged AlO_4^- exhibits four bands at 1039 (**A**), 1011 (**A′**), 685 (**C**), and 572 cm^{-1} (**D**). It looks rather similar to that of AlO_3^- suggesting a related geometry. The main difference is two bands instead of one band above 1000 cm^{-1}, which are also slightly red-shifted compared to the corresponding band in AlO_3^-. No experimental reference data for either neutral SiO_4 or group III tetraoxide anions are available in the literature. A highly symmetric (D_{2d}) $^1A_1$ ground state has been predicted for AlO_4^-, which is characterized by three IR-active bands in-between 400-1200 cm^{-1} instead of four that are observed in the present IRPD spectrum.[36] An assignment to a kite-like O–Al–O_3 structure, as predicted for GaO_4^-, is unlikely, as the most intense IR transition associated with this structure is expected at a lower energy (862 cm^{-1}), a region where no transition is observed in the IRPD spectrum of AlO_4^-.[63]

2. Dialuminum oxide anions

The IRPD spectra of $Al_2O_{3\text{-}6}^-$ (see Fig. 1) show considerably more IR activity compared to those of the mono-aluminum oxide anions, in particular in-between 700 and 950 cm^{-1}. The $Al_2O_{3\text{-}6}^-$ spectra share common features, including strong IR-activity near 850 cm^{-1} (band **C** and **D**) as well as two characteristic bands, labeled **G** and **H**, between 500 and 700 cm^{-1}, indicating that they share a common geometric motif. Previous APE spectra for $Al_2O_{2\text{-}5}^-$ reported by Desai *et al.*[18] found that this common motif is a Al–$(O)_2$–Al rhombic ring. Such cyclic structures have also been predicted for $B_2O_4^-$, $Ga_2O_{3\text{-}4}^-$, and the Si_2O_3.[62,64–66] The lower energy absorptions can then likely be assigned to various vibrational modes involving this four-membered ring.[67,68]

The previous APE study also suggested that $Al_2O_{3\text{-}5}^-$ exhibits terminal Al–O groups and, indeed, the IRPD spectra of $Al_2O_{3\text{-}5}^-$ are characterized by strong absorptions slightly above 1000 cm^{-1}, typical for the presence of such terminal Al–O groups. However, the number of IRPD bands observed (e.g., two for $Al_2O_3^-$) does not always correlate with the number of terminal Al—O groups expected (e.g., one for $Al_2O_3^-$), requiring further explanation (see below). No significant absorption is observed in this region for $Al_2O_6^-$, supporting the predicted O_2–Al–$(O)_2$–Al–O_2 structure, which contains two terminal η^2-O_2 groups but no terminal O-atoms.[7]

In more detail, the IRPD spectrum of $Al_2O_3^-\cdot D_2$ is characterized by five absorption features at 1076 (**A**), ~1019 (**A′**), ~818/800 (**C**/**D**), 629 (**G**), and 539 cm^{-1} (**H**). Four of these bands (**C**, **D**, **G**, and **H**) are also observed in the IRPD spectrum of $Al_2O_4^-\cdot D_2$. While no absorption corresponding to band **A** in the $Al_2O_3^-\cdot D_2$ spectrum is observed; however an additional intense feature appears at 913 cm^{-1} (**C**). The IRPD spectrum of $Al_2O_5^-\cdot D_2$ looks very similar to that of $Al_2O_4^-\cdot D_2$ with five bands at 1022 (**A**), ~907 (**C**), 851 (**D**), 650 (**G**), and 554 cm^{-1} (**H**), but no absorption in the vicinity of the weak feature **F** (715 cm^{-1}) observed for $Al_2O_4^-\cdot D_2$. Note, for $Al_2O_4^-$ and $Al_2O_5^-$ Desai *et al.*[18] reported features at low electron binding energies in the APE spectra that they assigned to hot bands involving vibrational modes at 1090 cm^{-1} ($Al_2O_4^-$) and 1170 cm^{-1} ($Al_2O_5^-$). We find no evidence of IR-active modes at such high energies, suggesting that these modes are either not IR-active or these features are of other origin. Finally, the IRPD spectrum of $Al_2O_6^-\cdot D_2$ resembles that of $Al_2O_5^-\cdot D_2$ with respect to the bands **C**, **D**, **G**, and **H**. It shows additional features at 937 (**B**), ~819 (**E**), and 729 cm^{-1} (**F**), and lacks any significant absorption above 950 cm^{-1}.

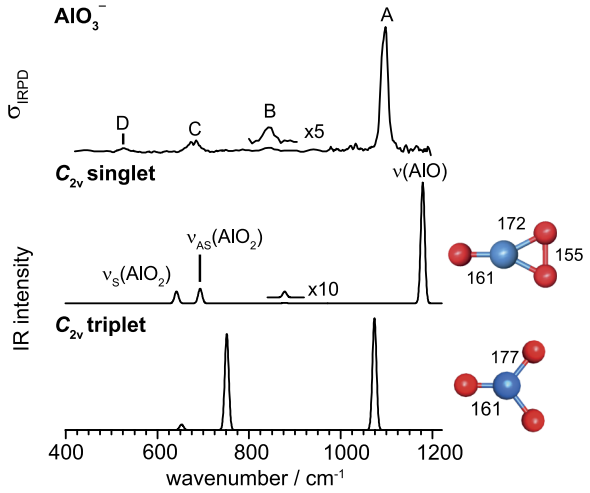

FIG. 2. IRPD spectrum of D_2-tagged AlO_3^- (top) compared to simulated IR spectra derived from harmonic BHLYP vibrational frequencies and intensities of low energy structures (Al = blue, O = red, bond lengths are in pm). Assignments of the IR-active vibrational modes are indicated (ν: stretch, ν_S/ν_{AS}: symmetric/antisymmetric stretch). See Table I for band positions and assignments.

B. Computational results

1. Monoaluminum oxide clusters $AlO_{1\text{-}4}^-$

AlO^- and AlO_2^- are electronic closed-shell systems and all three computational methods (B3LYP, BHLYP, and CCSD(T)) predict the same electronic and geometric structures. CCSD(T) and B3LYP vibrational frequencies are close to the experimental ones, while the BHLYP frequencies are blue-shifted (see Table I). Previous CCSD(T) calculations on AlO^- predicted a harmonic vibrational frequency of 969 cm^{-1} and an equilibrium bond length of 164 pm,[26] whereas our CCSD(T)/aCVTZ calculations yield values of 953 cm^{-1} and 165 pm, respectively. In AlO_2^-, the Al–O stretching mode is predicted higher (1127 cm^{-1}) and the bond distance is slightly shorter (164 pm).

For AlO_3^-, B3LYP and CCSD(T) calculations yield a closed-shell singlet ground state with a planar O–Al–O_2 structure of C_{2v} symmetry (see Fig. 2) containing a peroxo group (155 pm). In contrast, an open-shell species with three isolated oxygen atoms as part of a distorted D_{3h} structure (see Fig. 2) is predicted at slightly lower energy using BHLYP. Using B3LYP and CCSD(T), this species has significantly higher energies, 39 and 87 kJ/mol, see Fig. 3.

The harmonic IR spectra (BHLYP) of both of these structures are compared to the experimental IRPD spectrum in Fig. 2. The agreement is much better for the O–Al–O_2 structure (singlet state) than for the Al(–O)$_3$ structure (triplet state). For the O–Al–O_2 structure, the calculations yield three IR-active bands at 1179, 693, and 642 cm^{-1}. While the BHLYP frequencies are significantly blue-shifted by up to 120 cm^{-1} with respect to the experimentally observed IRPD bands **A**, **C**, and **D** (see Table I), the relative band positions and intensities agree favorably, supporting an assignment to the closed-shell C_{2v} structure. As in AlO^- and AlO_2^-, the terminal Al–O stretching mode of AlO_3^- is calculated highest in energy (1179 cm^{-1}). The two bands at lower energies then correspond to the antisymmetric and symmetric stretching mode of the Al–O_2 moiety (see Fig. 4). The intensity of the peroxide stretching mode at 878 cm^{-1} is found to be small (<1% relative intensity) by BHLYP. Indeed, we observe a small feature, labeled **B** in Fig. 2, at 842 cm^{-1} that could tentatively be attributed to this mode. Note, the CCSD(T) calculations (see Table I) predict the peroxide stretching mode at considerably lower energy (742 cm^{-1}).

For AlO_4^-, the genetic algorithm yields three low energy structures shown in Fig. 5. Fig. 3 (right panel) shows the relative stability of these structures as obtained with different methods. These are a D_{2d} structure containing two η^2-peroxo motifs, a planar C_{2v} structure containing an O_3 moiety (+14 kJ/mol), and a non-planar biradical C_s structure containing a single η^2-superoxo motif (+18 kJ/mol). The C_s structure may be considered as a superoxide radical $O_2^{-\cdot}$ coordinated to an asymmetric, bent AlO_2 radical with the extra electron localized on a single oxygen atom. In previous work,[36] the ground state structure was assumed to be a singlet state of D_{2d} symmetry, consistent with the B3LYP, BHLYP, and CCSD(T) results of this work.

There are two possible assignments for the experimental spectrum shown in Fig. 5: (i) The harmonic BHLYP results for the C_s structure may explain three of the four bands of the experimental IR spectrum. The calculated IR-active bands at 1081, 722, and 524 cm^{-1} which correspond to

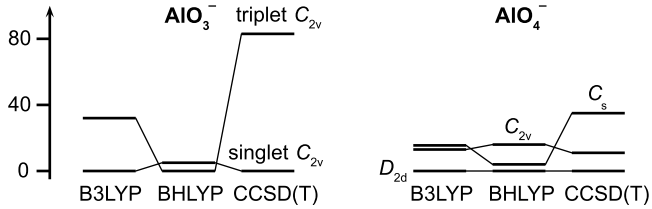

FIG. 3. Relative energies (in kJ/mol) of the low-energy isomers of AlO_3^- and AlO_4^- computed with different methods.

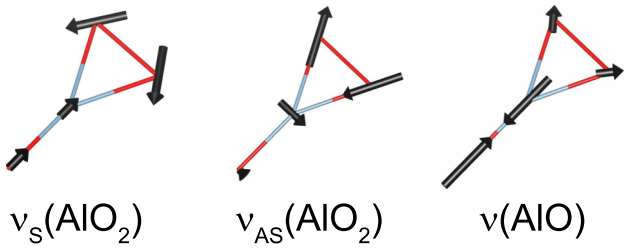

FIG. 4. Visualization of three normal modes (ν: stretch, ν_S/ν_{AS}: symmetric/antisymmetric stretch) of the closed-shell C_{2v} structure of AlO_3^-.

excitations of the Al–O stretch ν_1 involving the shorter Al–O· bond (161 pm), the Al–O stretch ν_2 of the longer Al–O bond (176 pm), and the symmetric stretch ν_S of the AlO_2 η^2-superoxo motif, respectively, can be assigned to bands **A**, **C,** and **D**, respectively. The fourth observed band **A′** may result from a Fermi resonance as anharmonic BHLYP calculations of the biradical C_s structure show (see Fig. 5). A resonance between the first overtone $2\nu_S$ and the ν_1 fundamental yields a doublet at 996 and 1068 cm^{-1} (see Fig. 5), which could be attributed to bands A′ and A, respectively. However, quantitative agreement for the band positions is not achieved.

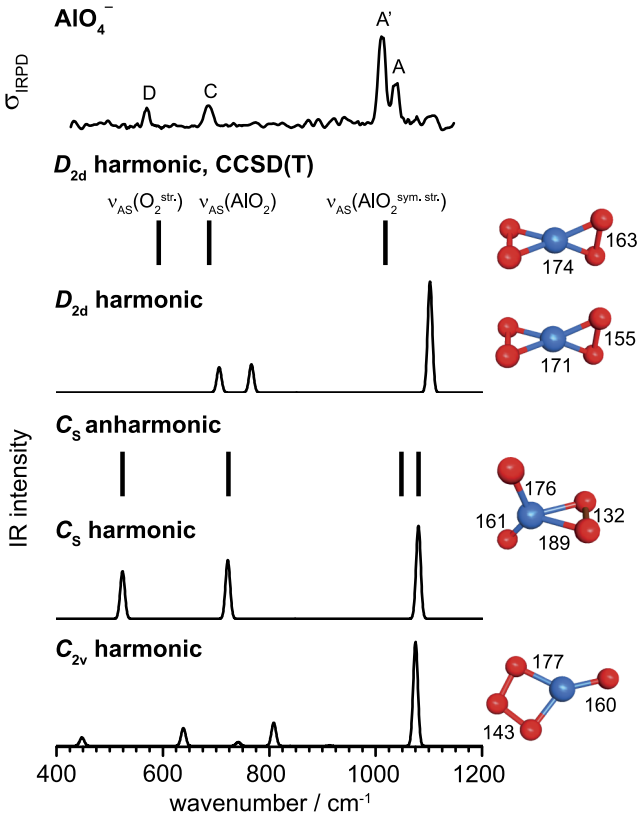

FIG. 5. IRPD spectrum of D_2-tagged AlO_4^- (top) compared to calculated IR spectra of low-energy structures (bond length are in pm) of AlO_4^-. The harmonic CCSD(T) stick spectrum (no intensities available) is shown beneath the experimental spectrum. All other panels show BHLYP results for different structures. Since intensities are not available the anharmonic BHLYP results for the C_s structure are also shown as stick spectrum. Assignments of the IR-active vibrational modes are indicated (ν_S/ν_{AS}: symmetric/antisymmetric stretch) and summarized together with experimental and calculated band positions in Table I. See text for details.

(ii) The harmonic CCSD(T) results of the D_{2d} structure for the band position are in very good agreement with the experiment. The most intense band **A′** at 1011 cm^{-1} is calculated at 1021 cm^{-1} and corresponds to $\nu_{AS}(AlO_2^{sym.\ str.})$, an antisymmetric combination (b_2) of the two AlO_2 symmetric stretches. The C and D bands at 685 and 572 cm^{-1} then are $\nu_{AS}(AlO_2)$, the two degenerate AlO_2 antisymmetric stretches (e), and $\nu_{AS}(O_2^{str.})$, the antisymmetric combination (b_2) of the two O_2 stretches, respectively, calculated at 683 cm^{-1} (e) and 587 cm^{-1} (b_2). Band **A** cannot be explained by a calculated fundamental transition. However, similar to the above discussed anharmonic spectrum of the C_s structure, the $\nu_S(AlO_2^{sym.\ str.}) + \nu_{AS}(O_2^{str.})$ combination band (see Table I) is expected close in energy to the $\nu_{AS}(AlO_2^{sym.\ str.})$ fundamental and could borrow intensity from it by way of Fermi coupling. B3LYP and BHLYP also show all these bands; however, the energetic ordering of the modes at 685 and 572 cm^{-1} (Bands **C** and **D**) is exchanged. The too high $\nu_{AS}(O_2^{str.})$ frequency is also reflected in a too short bond distance in BHLYP of 155 pm, compared to 163 pm in CCSD(T) (see Fig. 5). We therefore assign the IRPD spectrum of AlO_4^- to an electronically closed-shell D_{2d} structure, because (i) of the better agreement of the simulated spectrum with experiment and (ii) of its much lower CCSD(T) energy.

2. *Dialuminum oxide clusters $Al_2O_{3\text{-}6}^-$*

The BHLYP global minimum-energy structure of $Al_2O_3^-$ is a planar Al–(O_2)–Al ring with an exocyclic oxygen atom radical and overall C_{2v} symmetry, see Fig. 6. A non-cyclic C_{2v} isomer is found more than 100 kJ/mol higher in energy.

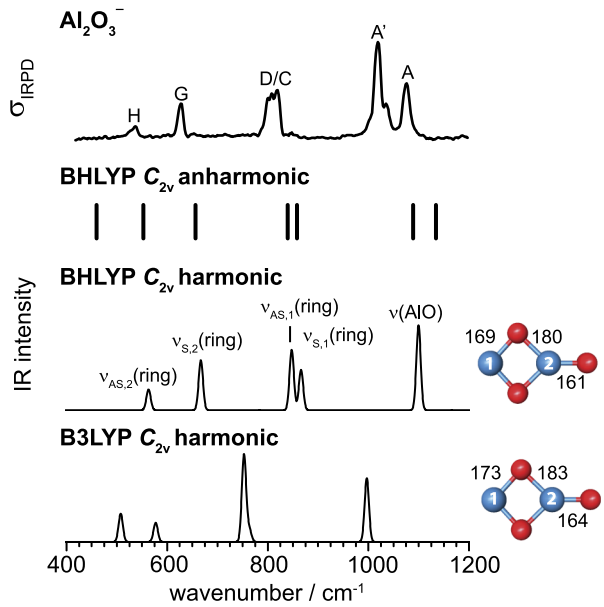

FIG. 6. IRPD spectrum of D_2-tagged $Al_2O_3^-$ (top) compared to simulated BHLYP anharmonic frequencies and harmonic IR spectrum of the minimum-energy structure (bond lengths in pm) of $Al_2O_3^-$. The B3LYP harmonic spectrum is also shown with the minimum structure. Assignments of the IR-active vibrational modes are indicated (ν: stretch, ν_S/ν_{AS}: symmetric/antisymmetric Al–(O_2) stretch, "1", and "2" refer to the doubly and triply coordinated Al-atom, respectively). See Table II for band positions and assignments.

Five of the six features observed in the IRPD spectrum of $Al_2O_3^-$ are reproduced by the harmonic BHLYP calculation (see Fig. 6). However, the most intense band **A′** at 1019 cm^{-1} is missing in the simulated spectrum. Band **A** corresponds to the stretching mode of the terminal Al–O group (harmonic 1099 cm^{-1}). Bands **C**, **D**, **G,** and **H** correspond to four characteristic modes involving the Al–$(O)_2$–Al ring, respectively. These four ring modes are observed for all di-aluminum oxide anions studied here. They are best visualized as symmetric and antisymmetric stretches of the Al–$(O)_2$ moieties involving one or the other Al-atom, labeled as $\nu_{S,1}$ (harmonic 866 cm^{-1}, **C**), $\nu_{AS,1}$ (harmonic 847 cm^{-1}, **D**), $\nu_{S,2}$ (harmonic 668 cm^{-1}, **G**), and $\nu_{AS,2}$ (harmonic 564 cm^{-1}, **H**) in Fig. 6, where the index 1 (2) refers to the doubly (triply) coordinated Al-atom in $Al_2O_3^-$. This leaves band **A′** unassigned, whose identity is revealed by the BHLYP anharmonic calculation (see Fig. 6). It results from Fermi-type coupling involving the overtone $2\nu_{AS,2}$, which borrows intensity from the intense ν(Al–O) stretch fundamental, resulting in anharmonic frequencies calculated at 1046 cm^{-1} (**A′**) and 1089 cm^{-1} (**A**).

The predicted structures of $Al_2O_4^-$ are strongly affected by the different balance of electron delocalization versus localization across the DFT functionals. Both BHLYP and B3LYP functionals predict an Al–$(O)_2$–Al ring with two terminal oxygen atoms and similar structural parameters, see Fig. 7. However, B3LYP yields a higher symmetric D_{2h} structure, which corresponds to an energetically high-lying local minimum in BHLYP, while BHLYP localizes the electron on one of the two terminal oxygen atoms, resulting in a more distorted C_{2v} structure. Consequently, the predicted harmonic spectra of these two structures are characteristically different, with the higher symmetry D_{2h} species yielding a much simpler IR spectrum with three instead of seven IR-active bands. For example, the symmetric stretching mode involving the two terminal Al–O bonds is IR-forbidden for the D_{2h} structure, but IR active for C_{2v} structure (1108 cm^{-1}). Indeed, the symmetry lowering induced by the electron localization with BHLYP results in an IR spectrum that qualitatively agrees with the experimental one (see Fig. 7) and allows assigning all six observed bands. Whereas bands **A** and **C** correspond to the terminal Al=O and Al–O stretching modes, respectively, bands **D**, **F**, **G**, and **H** correspond to the four characteristic ring deformation modes $\nu_{S,1}$, $\nu_{AS,1}$, $\nu_{S,2}$, and $\nu_{AS,2}$, respectively. Note, the different energetic ordering of the four ring modes for $Al_2O_4^-$ compared to $Al_2O_3^-$ which results from a pronounced coupling between the ν(Al–O) and $\nu_{S,1}$ mode, and red shifts the $\nu_{S,1}$ mode below 800 cm^{-1} in $Al_2O_4^-$. Furthermore, the rise in intensity observed at the edge of the experimental IRPD spectrum around 400 cm^{-1} is attributed to the band onset of a ring out-of-plane bending mode.

$Al_2O_5^-$ also contains an Al–$(O)_2$–Al ring with a terminal oxygen atom bound to one Al atom, and a superoxo group on the other Al atom. This removes the coupling between the ν(Al–O) and $\nu_{S,1}$(ring) mode, observed for $n = 4$, and restores the original energetic order of the four ring modes as in $Al_2O_3^-$ (and $Al_2O_6^-$). Similar to $Al_2O_4^-$, the charge delocalization of B3LYP yields a simulated spectrum that disagrees with the experimental one. Two very similar stable structures were found with BHLYP, namely, a peroxide and the superoxide structure. Their energies differ by less than 3 kJ/mol. The computed spectrum of the superoxide structure is in better agreement with the experimental one (see Fig. 8), indicating that this is the structure probed in the experiment. In particular, the distance between bands **A** and **C**, and the appearance of only the two bands **G** and **H** in the 850–500 cm^{-1} region, is well-reproduced by the calculation for the superoxide structure. The superoxide symmetric stretching mode is predicted at 1288 cm^{-1} with very low intensity (<1% relative intensity). We tentatively attribute it to the weak signal observed around 1113 cm^{-1} in the experimental spectrum, labeled "*" in Fig. 8.

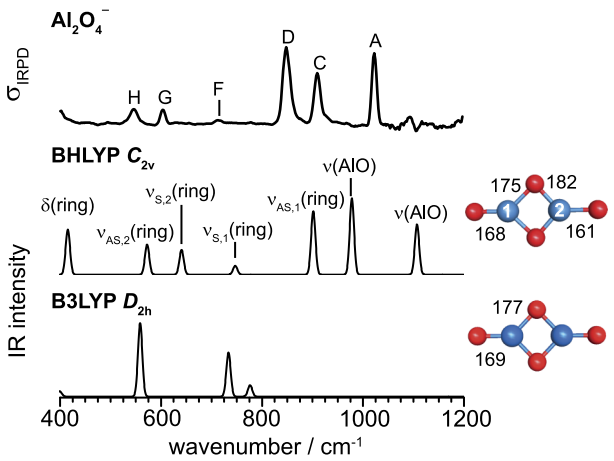

FIG. 7. IRPD spectrum of D_2-tagged $Al_2O_4^-$ (top) compared to simulated BHLYP harmonic IR spectrum of the C_{2v} minimum-energy structure (bond lengths in pm) of $Al_2O_4^-$. The B3LYP harmonic spectrum of the D_{2h} structure is also shown (see text). See Table II for band positions and assignments.

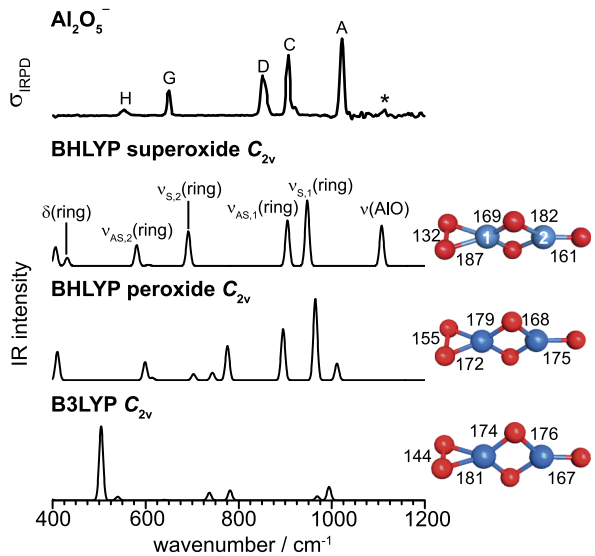

FIG. 8. IRPD spectrum of D_2-tagged $Al_2O_5^-$ (top) compared to simulated BHLYP harmonic IR spectrum of the superoxide C_{2v} minimum-energy structure (bond lengths in pm) of $Al_2O_5^-$. The BHLYP harmonic spectrum of the peroxide C_{2v} structure and the B3LYP harmonic spectrum of the C_{2v} structure are also shown (see text). See Table II for band positions and assignments. "*" denotes the weak absorption for O–O stretching.

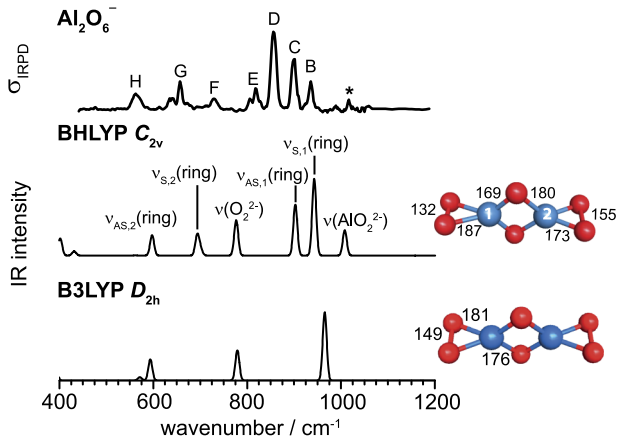

FIG. 9. Experimental IRPD spectrum of D_2-tagged $Al_2O_6^-$ (top) compared to simulated BHLYP harmonic IR spectrum of the C_{2v} minimum-energy structure (bond lengths in pm) of $Al_2O_6^-$. The B3LYP harmonic spectrum of the D_{2h} structure is also shown (see text). See Table II for band positions and assignments. "*" denotes the weak absorption for O–O stretching.

The C_{2v} structure shown in Fig. 9 represents the global minimum-energy structure of $Al_2O_6^-$ on the BHLYP PES. This structure is derived from that of $Al_2O_5^-$ by replacing the single oxygen atom with a peroxo group. Hence, this structure contains a stretched peroxo (155 pm) and a superoxo (132 pm) group. As for $Al_2O_4^-$, B3LYP yields a charge-delocalized D_{2h} structure, which represents an energetically higher lying minimum on the BHLYP PES.

Comparison of the simulated harmonic spectra with the experimental IRPD spectrum (see Fig. 9) supports an assignment to the C_{2v} structure. Bands **B** and **F** correspond to the Al–O_2 and O–O stretching modes involving the peroxo group. Bands **C**, **D**, **G**, and **H** are the four in-plane ring deformation modes $\nu_{S,1}$, $\nu_{AS,1}$, $\nu_{S,2}$, and $\nu_{AS,2}$, respectively. The superoxo stretching mode is calculated at 1287 cm^{-1} with little IR activity (<1% relative intensity). Similar to $Al_2O_5^-$, weaker features are indeed observed to the blue of the more intense IR transitions in the experimental spectrum. Band **E** has no counterpart in the simulated IR spectrum.[16]

C. Discussion

The common features observed in the IR spectra of small aluminum oxide clusters can be grouped in four spectral regions. Superoxo stretching modes are found at highest energies (1120-1010 cm^{-1}), but with very little IR intensity, complicating their identification. Peroxo modes are considerably lower in energy (850-570 cm^{-1}) and are predicted with slightly more IR intensity. Terminal Al–O stretching modes are found in the intermediate energy region (1140-960 cm^{-1}). The vibrational frequencies of superoxo, peroxo, and terminal Al–O groups are summarized in Table III.

The common structural motif of dialuminum oxide clusters is a four-membered Al–$(O)_2$–Al ring to which additional O-atoms add in an exocyclic manner, similar to other metal oxide clusters, e.g., vanadium oxides.[68] This ring is characterized by four IR active in-plane ring deformation modes between 910 and 530 cm^{-1}. The predicted energetic ordering is typically $\nu_{S,1}(ring) > \nu_{AS,1}(ring) > \nu_{S,2}(ring) > \nu_{AS,2}(ring)$ with wavenumber ranges of 910-710 cm^{-1} ($\nu_{S,1}$), 860-800 cm^{-1} ($\nu_{AS,1}$), 650-600 ($\nu_{S,2}$), and 560-530 cm^{-1} ($\nu_{AS,2}$). Out of plane bending modes are predicted below 400 cm^{-1}.

The electronic and geometric structures of the aluminum oxide clusters $Al_2O_{3-6}^-$ are governed by localization of the excess charge. In many cases, there is a competition between more symmetric structures with delocalized charge and less symmetric structures with more localized charge. As a consequence of charge localization, the electronic structures of the open-shell clusters $Al_2O_n^-$ are characterized by mixed valence.[51] Hence, the calculated electronic structure is very sensitive towards the amount of exact exchange that is mixed into the density functional. This is well known in the literature[51,69] and has been observed before, e.g., with the size-induced d-electron localization in polyhedral vanadium oxide anion cages[70] and the formation of electron holes in solid oxides.[71,72] The crossover point between DFT functionals with increasing amount of exact exchange for the physically correct description of the electronic structure depends on the observed system. In the present study, standard GGA functionals,

TABLE III. Experimental and calculated harmonic vibrational frequencies (in cm^{-1}) of different oxygen species in AlO_{1-4}^- and $Al_2O_{3-6}^-$, including irreducible representations (irrep) of the delocalized normal modes.

Species	Cluster	Expt.	Irrep	BHLYP (scaled)[a]	Bond Length
Superoxo	$Al_2O_5^-$	1113	a_1	1202	132
	$Al_2O_6^-$	1016	a_1	1202	132
Terminal Al–O	AlO_2^-	1134	σ_u	1159	163
	AlO_3^-	1098	a_1	1101	161
	$Al_2O_3^-$	1076	a_1	1026	161
	$Al_2O_4^-$	1024	a_1	1035	161
	$Al_2O_5^-$	1022	a_1	1032	161
	AlO^-	962	σ	971	164
Peroxo	$Al_2O_6^-$	729	a_1	726	155
	AlO_3^-	842	a_1	820	155
	AlO_4^-	572	b_2	716[b]	155[b]

[a]Scaled with 0.9339, taken from Table II of Ref. 73.
[b]CCSD(T) values: 587 cm^{-1} and 163 pm.

and also hybrid functional with the standard amount of Fock exchange, e.g., 20% for B3LYP, incorrectly predict the electronic structure to be delocalized and the geometric structure to be D_{2h} symmetric (if possible by stoichiometric composition). However, BHLYP (50% exchange) localizes the charge leading to a C_{2v} symmetric distortion. The surplus electron is localized on a terminal O-atom or O_2^- group, as indicated by bond lengths and population analyses and confirmed by the agreement of simulated and experimental spectra.

With the exception of AlO_3^-, the BHLYP functional (50% Fock exchange) provides a qualitatively correct description of all systems studied, although the calculated harmonic wavenumbers show a rather large rms deviation of 85 cm^{-1} for the 33 assigned wavenumbers in Tables I and II. Applying the global scale factor of 0.9339[73] the rms deviation is reduced to 45 cm^{-1}. If we use our data to derive a global scale factor, we obtain 0.919 with the rms value of 42 cm^{-1}.

V. SUMMARY

We have studied the structure and vibrational spectra of small aluminum oxide cluster anions. The structures were determined computationally by using a genetic algorithm for finding the global minimum and subsequently confirmed by comparison of the predicted spectra with measured IRPD spectra. The mononuclear species $AlO_{1,2}^-$ are linear, closed-shell molecules. AlO_3^- has a planar, triangular structure with a peroxo group, and AlO_4^- is a closed-shell D_{2d} symmetric molecule with two overstretched peroxo groups. The binuclear species $Al_2O_{3\text{-}6}^-$ are all open-shell doublets and oxygen-centered radicals. The common motif is a four-membered Al–(O_2)–Al ring, with one or two terminal oxo groups (n = 3,4), or with oxo/superoxo (n = 5) and peroxo/superoxo groups (n = 6). The electronic structure is characterized by the localization of the unpaired electron on one side of the cluster, lowering its symmetry from D_{2h} to C_{2v} (for n = 4,6). A correct description requires the use of density functionals with a large amount of Fock exchange such as BHLYP, otherwise the electron will delocalize and the vibrational spectra will not be reproduced.

ACKNOWLEDGMENTS

This research is supported by the Collaborative Research Center 1109 of the German Research Foundation DFG. We thank Professor Ludger Wöste for providing the magnetron sputter ion source. Xiaowei Song thanks the Alexander-von-Humboldt Foundation for a post-doctoral research fellowship. The authors also thank the reviewer for pointing out technical issues with the CCSD(T) calculations.

[1]M. Trueba and S. P. Trasatti, Eur. J. Inorg. Chem. **17**, 3393–3403 (2005).
[2]K. R. Asmis, Phys. Chem. Chem. Phys. **14**, 9270–9281 (2012).
[3]J. Sauer and H.-J. Freund, Catal. Lett. **145**, 109–125 (2015).
[4]D. K. Böhme and H. Schwarz, Angew. Chem., Int. Ed. **44**, 2336–2354 (2005).
[5]S. Feyel, J. Döbler, R. Höckendorf, M. K. Beyer, J. Sauer, and H. Schwarz, Angew. Chem., Int. Ed. **47**, 1946–1950 (2008).
[6]Z.-C. Wang, T. Weiske, R. Kretschmer, M. Schlangen, M. Kaupp, and H. Schwarz, J. Am. Chem. Soc. **133**, 16930–16937 (2011).
[7]L.-H. Tian, T.-M. Ma, X.-N. Li, and S.-G. He, Dalton Trans. **42**, 11205–11211 (2013).
[8]I. Cherchneff and E. Dwek, Astronom. J. **713**, 1–24 (2010).
[9]J. R. Scott, G. S. Groenewold, A. K. Gianotto, M. T. Benson, and J. B. Wright, J. Phys. Chem. A **104**, 7079–7090 (2000).
[10]G. E. Johnson, E. C. Tyo, and A. W. Castleman, Jr., J. Phys. Chem. A **112**, 4732–4735 (2008).
[11]R. Kretschmer, Z.-C. Wang, M. Schlangen, and H. Schwarz, Angew. Chem., Int. Ed. **52**, 9513–9517 (2013).
[12]S. B. H. Bach and S. W. McElvany, J. Phys. Chem. **95**, 9091–9094 (1991).
[13]L. V. Serebrennikov, S. B. Osin, and A. A. Maltsev, J. Mol. Struct. **81**, 25–33 (1982).
[14]S. M. Sonchik, L. Andrews, and K. D. Carlson, J. Phys. Chem. **87**, 2004–2011 (1983).
[15]S. J. Bares, M. Haak, and J. W. Nibler, J. Chem. Phys. **82**, 670–675 (1985).
[16]G. Stößer and H. Schnöckel, Angew. Chem., Int. Ed. **44**, 4261–4264 (2005).
[17]S. R. Desai, H. Wu, and L.-S. Wang, Int. J. Mass Spectrom. **159**, 75–80 (1996).
[18]S. R. Desai, H. Wu, C. M. Rohlfing, and L.-S. Wang, J. Chem. Phys. **106**, 1309–1317 (1997).
[19]G. Meloni, M. J. Ferguson, and D. M. Neumark, Phys. Chem. Chem. Phys. **5**, 4073–4079 (2003).
[20]F. A. Akin and C. C. Jarrold, J. Chem. Phys. **118**, 5841–5851 (2003).
[21]M. Sierka, J. Döbler, J. Sauer, H. J. Zhai, and L. S. Wang, ChemPhysChem **10**, 2410–2413 (2009).
[22]K. J. Mascaritolo, A. M. Gardner, and M. C. Heaven, J. Chem. Phys. **143**, 114311 (2015).
[23]G. Santambrogio, E. Janssens, S. Li, T. Siebert, G. Meijer, K. R. Asmis, J. Döbler, M. Sierka, and J. Sauer, J. Am. Chem. Soc. **130**, 15143–15149 (2008).
[24]E. F. Archibong and A. St-Amant, J. Phys. Chem. A **102**, 6877–6882 (1998).
[25]E. F. Archibong and A. St-Amant, J. Phys. Chem. A **103**, 1109–1114 (1999).
[26]G. L. Gutsev, P. Jena, and R. J. Bartlett, J. Chem. Phys. **110**, 2928–2935 (1999).
[27]A. Martínez, F. J. Tenorio, and J. V. Ortiz, J. Phys. Chem. A **105**, 11291–11294 (2001).
[28]A. B. C. Patzer, C. Chang, E. Sedlmayr, and D. Sülzle, Eur. Phys. J. D **32**, 329–337 (2005).
[29]A. V. Nemukhin and J. Almlof, J. Mol. Struct.: THEOCHEM **85**, 101–107 (1992).
[30]A. V. Nemukhin and F. Weinhold, J. Chem. Phys. **97**, 3420–3430 (1992).
[31]A. B. C. Patzer, C. Chang, E. Sedlmayr, and D. Sülzle, Eur. Phys. J. D **6**, 57–62 (1999).
[32]S. Neukermans, N. Veldeman, E. Janssens, P. Lievens, Z. Chen, and P. v. R. Schleyer, Eur. Phys. J. D **45**, 301–308 (2007).
[33]S. M. Woodley, Proc. R. Soc. A **467**, 2020–2042 (2011).
[34]A. B. Rahane, M. D. Deshpande, and V. Kumar, J. Phys. Chem. C **115**, 18111–18121 (2011).
[35]M. I. M. Sarker, C. S. Kim, and C. H. Choi, Chem. Phys. Lett. **411**, 297–301 (2005).
[36]E. F. Archibong, N. Seeburrun, and P. Ramasami, Chem. Phys. Lett. **481**, 169–172 (2009).
[37]G. L. Gutsev, C. A. Weatherford, K. Pradhan, and P. Jena, J. Comput. Chem. **32**, 2974–2982 (2011).
[38]D. J. Goebbert, E. Garand, T. Wende, R. Bergmann, G. Meijer, K. R. Asmis, and D. M. Neumark, J. Phys. Chem. A **113**, 7584–7592 (2009).
[39]I. M. Goldby, B. von Issendorff, L. Kuipers, and R. E. Palmer, Rev. Sci. Instrum. **68**, 3327–3334 (1997).
[40]See supplementary material at http://dx.doi.org/10.1063/1.4954158 for additional experimental (mass spectrum, effect of mutiple messenger tags) and computational (total energies and structures) results.
[41]W. Schöllkopf, S. Gewinner, H. Junkes, A. Paarmann, G. von Helden, H. Bluem, and A. M. M. Todd, Proc. SPIE **9512**, 95121L (2015).
[42]N. Heine and K. R. Asmis, Int. Rev. Phys. Chem. **34**, 1–34 (2015).
[43]M. Sierka, Prog. Surf. Sci. **85**, 398–434 (2010).
[44]M. Sierka, J. Döbler, J. Sauer, G. Santambrogio, M. Brümmer, L. Wöste, E. Janssens, G. Meijer, and K. R. Asmis, Angew. Chem., Int. Ed. **46**, 3372–3375 (2007).
[45]J. P. Perdew, Phys. Rev. B **33**, 8822–8824 (1986).
[46]A. D. Becke, Phys. Rev. A **38**, 3098–3100 (1988).
[47]F. Weigend and R. Ahlrichs, Phys. Chem. Chem. Phys. **7**, 3297–3305 (2005).
[48]A. D. Becke, J. Chem. Phys. **98**, 5648 (1993).
[49]TURBOMOLE V6.5 2013, a development of University of Karlsruhe and Forschungszentrum Karlsruhe GmbH, 1989-2007, TURBOMOLE GmbH, since 2007; available from http://www.turbomole.com.

[50]A. D. Becke, J. Chem. Phys. **98**, 1372 (1993).
[51]K. Raghavachari, G. W. Trucks, J. A. Pople, and M. Head-Gordon, Chem. Phys. Lett. **157**, 479–483 (1989).
[52]K. A. Peterson and T. H. Dunning, J. Chem. Phys. **117**, 10548 (2002).
[53]M. Sierka, B. Helmich, and R. Wlodarczyk, *Program DoDo* (Humboldt University Berlin, Friedrich-Schiller University Jena, 2013).
[54]V. Barone, J. Chem. Phys. **122**, 14108 (2005).
[55]H.-J. Werner, P. J. Knowles, G. Knizia, F. R. Manby, and M. Schütz, Wiley Interdiscip. Rev.: Comput. Mol. Sci. **2**, 242–253 (2012).
[56]M. J. Frisch, G. W. Trucks, H. B. Schlegel, G. E. Scuseria, M. A. Robb, J. R. Cheeseman, G. Scalmani, V. Barone, B. Mennucci, G. A. Petersson, H. Nakatsuji, M. Caricato, X. Li, H. P. Hratchian, A. F. Izmaylov, J. Bloino, G. Zheng, J. L. Sonnenberg, M. Hada, M. Ehara, K. Toyota, R. Fukuda, J. Hasegawa, M. Ishida, T. Nakajima, Y. Honda, O. Kitao, H. Nakai, T. Vreven, J. A. Montgomery, Jr., J. E. Peralta, F. Ogliaro, M. Bearpark, J. J. Heyd, E. Brothers, K. N. Kudin, V. N. Staroverov, R. Kobayashi, J. Normand, K. Raghavachari, A. Rendell, J. C. Burant, S. S. Iyengar, J. Tomasi, M. Cossi, N. Rega, J. M. Millam, M. Klene, J. E. Knox, J. B. Cross, V. Bakken, C. Adamo, J. Jaramillo, R. Gomperts, R. E. Stratmann, O. Yazyev, A. J. Austin, R. Cammi, C. Pomelli, J. W. Ochterski, R. L. Martin, K. Morokuma, V. G. Zakrzewski, G. A. Voth, P. Salvador, J. J. Dannenberg, S. Dapprich, A. D. Daniels, Ö. Farkas, J. B. Foresman, J. V. Ortiz, J. Cioslowski, and D. J. Fox, GAUSSIAN 09, Gaussian, Inc., Wallingford CT, 2009.
[57]L. Andrews and M. McCluskey, J. Mol. Spectrosc. **154**, 223–225 (1992).
[58]S. Gowtham, A. Costales, and R. Pandey, J. Phys. Chem. B **108**, 17295–17300 (2004).
[59]H.-J. Zhai, L.-M. Wang, S.-D. Li, and L.-S. Wang, J. Phys. Chem. A **111**, 1030–1035 (2007).
[60]B. Tremblay, P. Roy, L. Manceron, M. E. l. Alikhani, and D. Roy, J. Chem. Phys. **104**, 2773 (1996).
[61]A. Beste and R. J. Bartlett, Chem. Phys. Lett. **366**, 100–108 (2002).
[62]S. Gowtham, M. Deshpande, A. Costales, and R. Pandey, J. Phys. Chem. B **109**, 14836–14844 (2005).
[63]E. F. Archibong and P. Ramasami, Comput. Theor. Chem. **964**, 324–328 (2011).
[64]P. V. Avramov, I. Adamovic, K.-M. Ho, C. Z. Wang, W. C. Lu, and M. S. Gordon, J. Phys. Chem. A **109**, 6294–6302 (2005).
[65]A. B. Rahane and M. D. Deshpande, J. Phys. Chem. C **116**, 2691–2701 (2012).
[66]A. K. Kandalam, B. Kiran, P. Jena, S. Pietsch, and G. Ganteför, Phys. Chem. Chem. Phys. **17**, 26589–26593 (2015).
[67]E. F. Archibong and E. N. Mvula, Chem. Phys. Lett. **408**, 371–376 (2005).
[68]K. R. Asmis, G. Meijer, M. Brümmer, C. Kaposta, G. Santambrogio, L. Wöste, and J. Sauer, J. Chem. Phys. **120**, 6461–6470 (2004).
[69]M. Sodupe, J. Bertran, L. Rodriguez-Santiago, and E. J. Baerends, J. Phys. Chem. A **103**, 166–170 (1999).
[70]K. R. Asmis, G. Santambrogio, M. Brümmer, and J. Sauer, Angew. Chem., Int. Ed. **44**, 3122–3125 (2005).
[71]G. Pacchioni, F. Frigoli, D. Ricci, and J. A. Weil, Phys. Rev. B **63**, 054102 (2001).
[72]X. Solans-Monfort, V. Branchadell, M. Sodupe, M. Sierka, and J. Sauer,J. Chem. Phys. **121**, 6034–6041 (2004).
[73]J. P. Merrick, D. Moran, and L. Radom, J. Phys. Chem. A **111**, 11683–11700 (2007).